Surface Air Temperature Simulations by AMIP General Circulation Models: Volcanic and ENSO Signals and Systematic Errors

JIANPING MAO AND ALAN ROBOCK*

Department of Meteorology, University of Maryland, College Park, Maryland

(Manuscript received 12 February 1996, in final form 13 August 1997)

ABSTRACT

Thirty surface air temperature simulations for 1979–88 by 29 atmospheric general circulation models are analyzed and compared with the observations over land. These models were run as part of the Atmospheric Model Intercomparison Project (AMIP). Several simulations showed serious systematic errors, up to 4°–5°C, in globally averaged land air temperature. The 16 best simulations gave rather realistic reproductions of the mean climate and seasonal cycle of global land air temperature, with an average error of −0.9°C for the 10-yr period. The general coldness of the model simulations is consistent with previous intercomparison studies. The regional systematic errors showed very large cold biases in areas with topography and permanent ice, which implies a common deficiency in the representation of snow-ice albedo in the diverse models. The SST and sea ice specification of climatology rather than observations at high latitudes for the first three years (1979–81) caused a noticeable drift in the neighboring land air temperature simulations, compared to the rest of the years (1982–88). Unsuccessful simulation of the extreme warm (1981) and cold (1984–85) periods implies that some variations are chaotic or unpredictable, produced by internal atmospheric dynamics and not forced by global SST patterns.

Among the 16 best simulations, 8 reproduced the dominant El Niño–Southern Oscillation (ENSO) mode in the 10-yr period, which includes the 1982–83 and 1986–87 warm episodes and the 1988 cold episode. On the average, the ENSO mode explains about 30% of the total variance in surface air temperature fluctuation and has a 2-month lag from the Southern Oscillation index. In this mode, North America displays a Pacific–North American–like anomaly pattern, but Eurasia gave little response to warm SSTs in the eastern equatorial Pacific, in good agreement with results based on historical data.

The special design of the AMIP experiment provides a unique opportunity to estimate the effects of the El Chichón volcanic eruption in spring 1982, which was not included in the model forcing. Comparison of the simulations with data delineated a visible global cooling in the first months following the El Chichón eruption, in addition to the cooling from the volcanic eruption of Nyamuragira in December 1981, due to the reduction of incoming solar radiation by volcanic aerosols. However, the mean climate shift in the AMIP experiment due to the forcing data discontinuity at the end of 1981 made the quantitative estimate of El Chichón global cooling influence impossible. The contrast between the simulated ENSO signal and observations shows that the major warming over the northern continents during the 1982/83 winter (DJF) is not an ENSO-like signal. Instead it is most likely a pattern resulting from the enhanced polar vortex produced by a larger pole-to-equator temperature gradient. This gradient was due to the larger absorption of radiation in low latitudes by the El Chichón volcanic sulfate aerosols in the stratosphere. These results suggest that during the Northern Hemisphere wintertime, the stratospheric polar vortex has substantial influence on surface air temperature fluctuations through its effects on vertically propagating planetary waves of the troposphere, and imply that current GCMs are deficient in simulation of stratospheric processes and their coupling with the troposphere.

1. Introduction

The Atmospheric Model Intercomparison Project (AMIP; Gates 1992a) was conducted for the period 1979–88, in which one of the largest volcanic eruptions of the century, El Chichón in April 1982, occurred (Robock 1983). In addition, three El Niño–Southern Oscillation (ENSO) events took place, the 1982–83 "the El Niño of the century," the 1986–87 El Niño, and the 1988 La Niña. The sulfur-rich emissions of the volcanic eruption produced a dense stratospheric sulfate aerosol veil in the Northern Hemisphere (Rampino and Self 1984), reducing the incoming solar radiation and generally cooling the earth's surface. Interpretation of the resulting climate effects of the eruption was complicated due to the coincident El Niño, which caused warmer tropical sea surface temperatures (SSTs) and masked the expected general cooling signal from the eruption. While a major winter warming over northern continents

* Current affiliation: Department of Environmental Sciences, Rutgers–The State University, New Brunswick, New Jersey.

Corresponding author address: Jianping Mao, Raytheon STX Corporation, 4400 Forbes Blvd., Lanham, MD 20706.
E-mail: mao@stx.com

would be expected following the large volcanic eruption, based on historical data composites (Robock and Mao 1992, 1995), atmospheric general circulation model (AGCM) simulations (Graf et al. 1993), and data analysis (Kodera 1994), the coincident El Niño complicated the assessment of the warming signal during the 1982/83 Northern Hemisphere (NH) winter (December–February, DJF) because the El Niño probably also introduced a large warming over extratropical land, at least over North America.

In the AMIP 10-yr runs, all the atmospheric models were forced by observed SSTs, and used the same values of CO_2 concentration and solar constant, but did not include any in situ atmospheric forcing due to changing greenhouse gases and aerosol concentration during the period. The observed SSTs, of course, include the results of the in situ forcing as reflected in their effects on SSTs, so the climate change in the model simulations is the result of forcing by the SST anomalies induced by the volcanic eruption and anthropogenic forcing, but not directly caused by the forcing in the atmosphere. For the first two or three years after a large volcanic eruption, such as the El Chichón eruption or the Mount Pinatubo eruption in 1991, the radiative forcing of volcanic sulfate aerosols is larger than the simultaneous forcing from the change of all anthropogenic greenhouse gases (Hansen et al. 1992), so we would expect that during the time it takes for the oceans to respond, the actual temperature of the earth would differ from the AMIP simulation output. We decided to take advantage of the design of the AMIP experiment to see whether the signal from the El Chichón eruption could be detected in the difference between the output from the AMIP models and the actual observations.

AMIP offers an unprecedented opportunity for the comprehensive evaluation and validation of current atmospheric models (Gates 1992a). One basic purpose of this project is to determine models' systematic errors on seasonal and interannual timescales in order to narrow the uncertainties of climate modeling. Surface air temperature is the most common and classical meteorological parameter to indicate climate change resulting from either internal processes, such as air–sea interaction, or external forcing, such as the change of greenhouse gas concentrations and volcanic aerosols. In this study, we first examine the systematic errors of the surface air temperature simulations and the dominant ENSO mode in the interannual variations. Then the influences of the El Chichón eruption on both global cooling and regional winter warming (Robock and Mao 1992) are examined by the difference between the model simulations and the data and comparisons to previous historical analysis.

A shorter preliminary version of this paper was published as Mao and Robock (1995).

2. Data and model simulations

To compare to the model simulations, we use a global $2°$ lat $× \ 2.5°$ long gridded monthly mean surface air temperature dataset (Schemm et al. 1992), one of the standard AMIP validation datasets (Gates 1994). The data came from the world monthly surface station climatology dataset (Spangler and Jenne 1990) obtained from the National Center for Atmospheric Research (NCAR). The interpolation from the station data to grid data was performed by averaging station values within a 300-km radius of each grid point with weights proportional to the inverse of the square of the distances of the stations from the grid point. The grid point has missing values if there are no station data within the 300-km radius. This dataset is from land stations only. Since the AMIP simulation is forced by observed monthly mean SSTs, the surface air temperatures over oceans are almost identical for each model archive. Therefore, we only need to analyze the simulations over land and compare them with the data. All the comparisons of the simulations with the data in this study are based on the same spatial coverage as the data and only for land; that is, the spatial averages from model output are only for the grid points that also have observations.

The AMIP experimental design required that all modeling groups submit, as standard output, monthly average gridpoint values of 57 variables (Gates 1992b) for the 10-yr period 1979–88, one of which is surface air temperature. There are 30 modeling groups from around the world participating in AMIP; the acronyms hereafter used are defined in Table 1. Thirty surface air temperature simulations from 29 modeling groups (two from ECMWF with different initial conditions) are available. Phillips (1994) describes the models in detail. The horizontal resolution of the models ranges from $2.5°$ lat $×$ $3.75°$ long to $4°$ lat $× 5.625°$ long grids among the finite-difference models, and from R15/T21 to R40/T63 among the spectral models. Almost all of the models have coarser resolution than the data, so we regridded the simulations onto the same grid as the data, $2°$ $×$ $2.5°$, by using bilinear interpolation, and made all the comparisons on this same grid.

3. Results

a. Means

As an overall evaluation of the models' performance in surface air temperature simulation, the globally averaged (over the grid points where there are observations) land air temperatures from the total 30 available AMIP simulations are examined. We found that several simulations (e.g., CSU, IAP, MGO, and YONU) had serious systematic errors, of up to $4°–5°C$, compared to the data (Fig. 1). The major problems are in the models themselves, such as inadequate representation of physical processes, or poor vertical resolution near the surface. A contributing factor may be that the surface air temperature output was not specified at the 2-m standard reference level (P. Glecker 1995, personal communication). For example, the output from GFDL supplied

TABLE 1. AMIP modeling groups.

Acronym	AMIP Group	Location
BMRC	Bureau of Meteorology Research Centre	Melbourne, Australia
CCC	Canadian Centre for Climate Modelling and Analysis	Victoria, Alberta, Canada
CNRM	Centre National de Recherches Météorologiques	Toulouse, France
COLA	Center for Ocean–Land–Atmosphere Studies	Calverton, Maryland
CSIRO	Commonwealth Scientific and Industrial Research Organisation	Mordialloc, Australia
CSU	Colorado State University	Fort Collins, Colorado
DERF	Dynamical Extended Range Forecasting (at GFDL)	Princeton, New Jersey
DNM	Department of Numerical Mathematics (of the Russian Academy of Sciences)	Moscow, Russia
ECMWF	European Centre for Medium-Range Weather Forecasts	Reading, United Kingdom
ECMWF2	European Centre for Medium-Range Weather Forecasts (with different initial conditions)	Reading, United Kingdom
GFDL	Geophysical Fluid Dynamics Laboratory	Princeton, New Jersey
GISS	Goddard Institute for Space Studies	New York, New York
GLA	Goddard Laboratory for Atmospheres	Greenbelt, Maryland
GSFC	Goddard Space Flight Center	Greenbelt, Maryland
IAP	Institute of Atmospheric Physics (of the Chinese Academy of Sciences)	Beijing, China
JMA	Japan Meteorological Agency	Tokyo, Japan
LMD	Laboratoire de Météorologie Dynamique	Paris, France
MGO	Main Geophysical Observatory	St. Petersburg, Russia
MPI	Max-Planck-Institut für Meteorologie	Hamburg, Germany
MRI	Meteorological Research Institute	Ibaraki-ken, Japan
NCAR	National Center for Atmospheric Research	Boulder, Colorado
NMC	National Meteorological Center*	Suitland, Maryland
NRL	Naval Research Laboratory	Monterey, California
RPN	Recherche en Prévision Numérique	Dorval, Quebec, Canada
SUNYA	State University of New York at Albany	Albany, New York
SUNYA–NCAR	State University of New York at Albany–National Center for Atmospheric Research	Albany, New York Boulder, Colorado
UCLA	University of California, Los Angeles	Los Angeles, California
UIUC	University of Illinois at Urbana–Champaign	Urbana, Illinois
UKMO	United Kingdom Meteorological Office	Bracknell, United Kingdom
YONU	Yonsei University	Seoul, Korea

* Now known as the National Centers for Environmental Prediction.

to AMIP is the temperature at 990 mb, the lowest model level, which results in a general cold bias (R. Wetherald 1995, personal communication). This bias, however, would be less than 1°C and could not completely account for the large errors shown in Fig. 1. The output provided by RPN is actually the ground temperature due to a mistake in the data transmission (B. Dugas 1995, personal communication). Thus, serious biases will be expected when such output is compared with surface air temperature observations. Unfortunately, the specific method of calculating surface air temperature output for every model group has not been completely documented (P. Glecker 1995, personal communication).

Figure 2 shows the global average temperature anomalies for each model and the data, after removing the mean seasonal cycle, which shows several interesting features. First, the summer of 1982 is the only time in the entire 10 yr when all models are warmer than the observations, perhaps an indication of the effect of the El Chichón eruption of early April 1982, which is discussed in more detail later. Several of the models have obvious spinup problems at the beginning of the runs, most notably BMRC, CSU, DERF, MGO, NMC, and UKMO. This is related, in many cases, to their improper

soil moisture initialization, as discussed by Robock et al. (1998). As mentioned above, the RPN results have no interannual variations, indicating an error in the transmission of the surface temperature results.

Since accurate simulation of interannual variations (e.g., the ENSO signal) depends on an accurate simulation of the mean climate (Houghton et al. 1990), it is necessary to filter out the simulations with serious systematic errors for further studies of climate variations. We could have removed the biases from all models and just analyzed the resulting anomalies, but if the wrong physical quantity was reported, it would not perform as atmospheric temperature. If the bias was actually in surface air temperature, a large bias could produce erroneous feedback in the climate system. Therefore, we eliminated all models with large biases from further analyses. Among the 30 simulations, the root-mean-square errors of monthly global-mean land air temperature for the 10-yr period ranged from 0.7°C to 4.1°C, with an average of about 2°C. In the following analyses, we chose only 16 of the 30 simulations that had a root-mean-square error less than 2°C to study the mean systematic errors of the simulations and their variabilities. These are the simulations of CNRM, CSIRO, DERF,
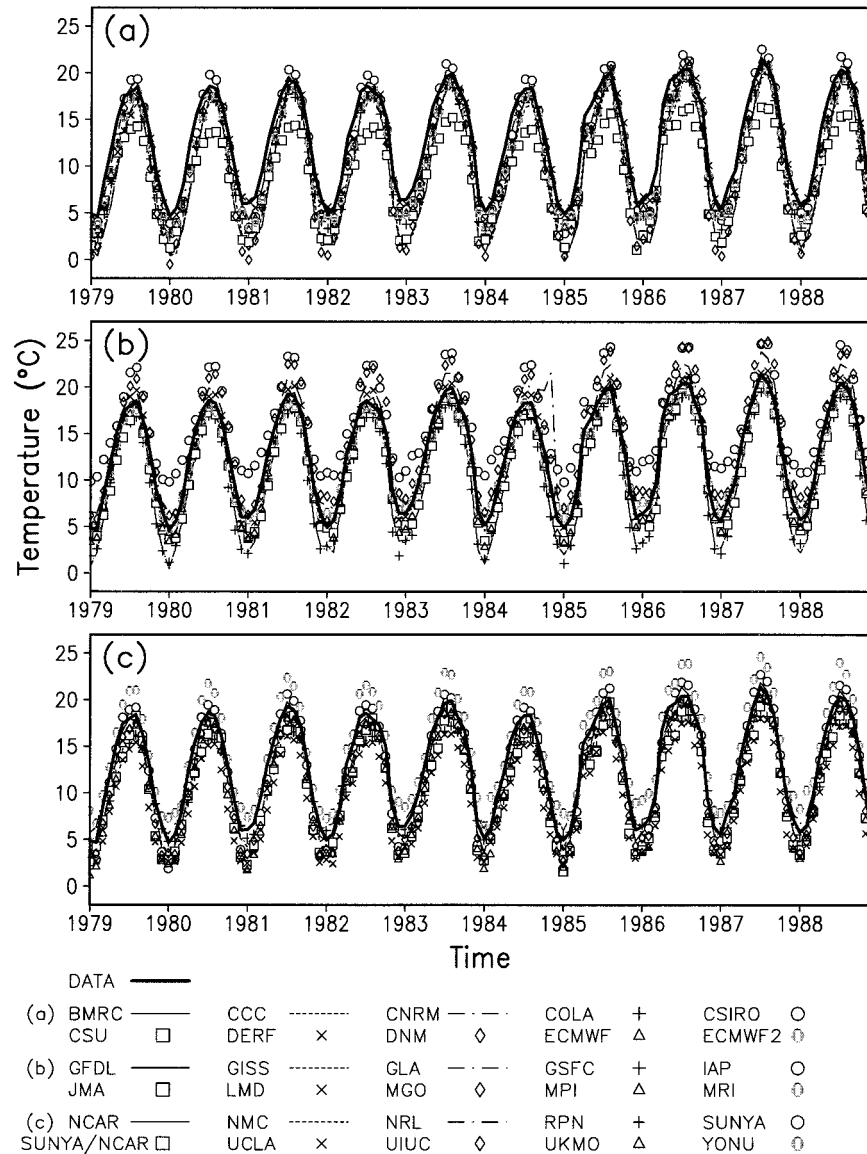
FIG. 1. Monthly mean, global land air temperatures for the 1979–88 period for the 30 AMIP simulations (Table 1) and observational data (Schemm et al. 1992). The years on the abscissa are plotted for January of the particular year.

ECMWF, ECMWF2, GISS, GLA, JMA, LMD, MPI, MRI, NCAR, NMC, NRL, SUNYA–NCAR, and UIUC.

Figure 3 shows that the average of the 16 model simulations gave a realistic mean climate and realistic seasonal cycles of globally averaged land air temperature. Generally, the simulated temperatures are colder than observed temperatures, with an average bias of −0.9°C for the 10-yr period and a maximum error of −2.2°C. This general coldness of GCM simulations has also been found in previous model intercomparison studies (e.g., Boer et al. 1992). This remarkable and robust feature of the models, despite their marked differences in resolution and the diversity of their physical parameteri-

zations, suggests that current models suffer from a common deficiency in some aspect of their formulation.

The monthly mean errors in the bottom panel of Fig. 3 show 0.7°C and 1.0°C cooling in April and May 1982 individually, soon after the El Chichón eruption, compared to that in March 1982. These temperature depressions perhaps indicate the global cooling effect of El Chichón eruption. However, from the biases of the simulations to observations, this result is uncertain due to common large cold biases in April and May for the other nine years.

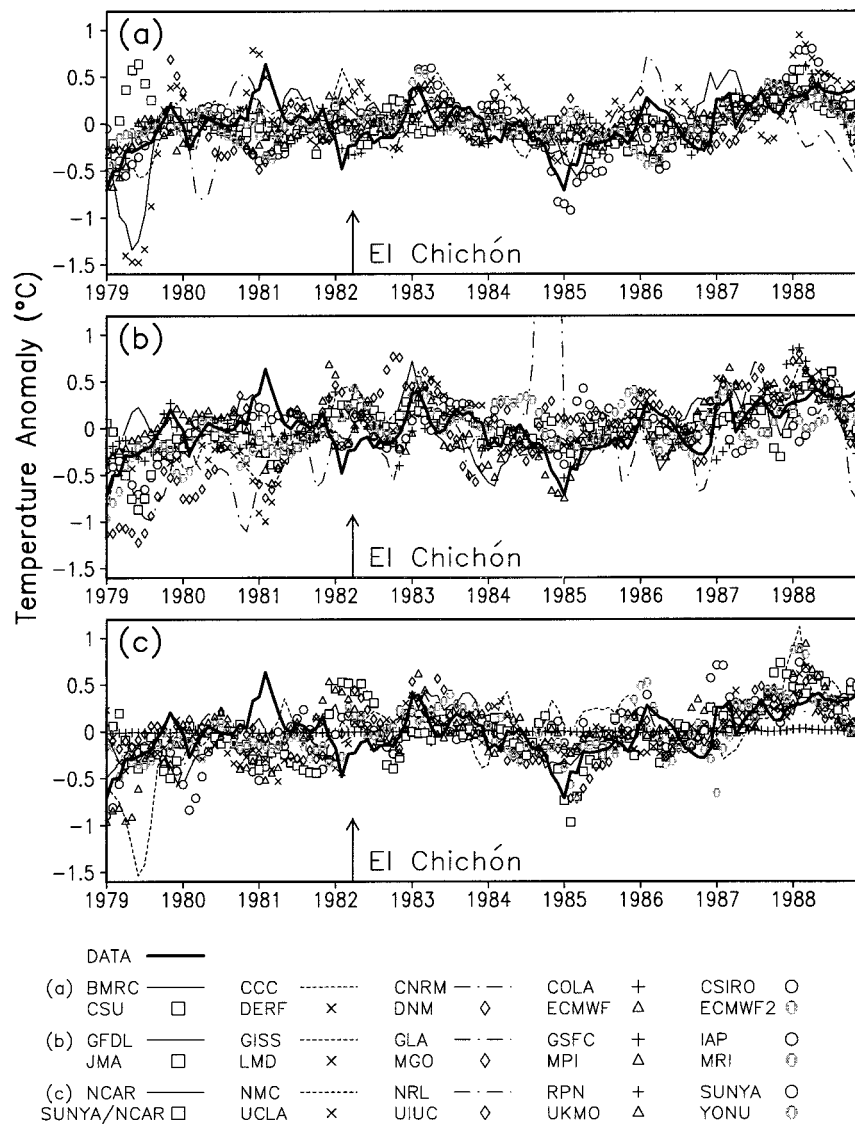The annual mean errors in the bottom panel of Fig. 3 show a noticeable jump (~0.4°C) from the first three

FIG. 2. Anomalies of the 30 AMIP simulations and the observations of monthly mean global land air temperatures, relative to the 1979–88 means for each month for each model and the data. The curves are smoothed with a 3-month running mean. The years on the abscissa are plotted for January of the particular year.

years (1979–81) to the last seven years (1982–88). This jump is because the SSTs and sea ice data used for AMIP for 1979–81 were in situ observations from ships and buoys only for 40°S–50°N and climatological means poleward of 40°S and 50°N, but for 1982–88 the data were the Reynolds blended SST analysis in which in situ observations combined with satellite observations (Reynolds 1988) were used for the whole globe (M. Fennessy and R. Reynolds 1995, personal communication). This jump is mostly related to the discontinuity of the sea ice dataset at the end of 1981 (Hansen et al. 1996). Larger sea ice area in the first three years (Hansen et al. 1996) apparently resulted in the colder globally averaged land surface temperatures (shown in Fig. 3).

There is another discontinuity of the sea ice dataset at the end of 1987 (Hansen et al. 1996), however, the influence of this discontinuity is very slight in Fig. 3. As expected, the effects of these SST forcing shifts on land surface air temperature are mostly confined to the high latitudes adjacent to the sea ice. The jump in the mean climate and the consequent climate perturbation could be eliminated by using a reanalysis of SSTs in future AMIP II experiments.

The general coldness of the simulations is relatively larger from NH winter to early summer (Fig. 4). In fact, the simulations have large regional errors (Fig. 5), even though their global means seem to be close to the data. The large cold biases are located in the mountainous

Global Land Air Temperature

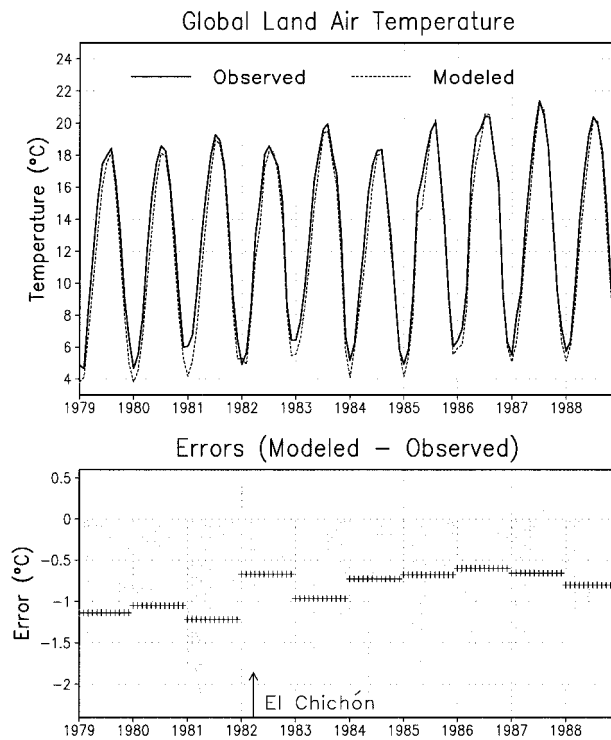
Errors (Modeled − Observed)

FIG. 3. The 1979–88 time series of monthly mean global land air temperatures averaged for the 16 selected AMIP simulations and as observed in the upper panel, and average monthly and annual mean errors of the simulations relative to the observations in the bottom panel. The years on the abscissa are plotted for January of the particular year.
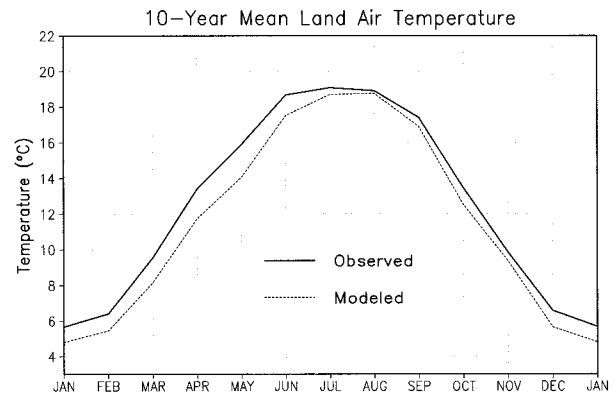
10-Year Mean Land Air Temperature

FIG. 4. Seasonal cycle of average observed and simulated monthly mean global land air temperature for the 16 selected AMIP simulations.

areas, such as the Rocky Mountains, the Tibetan Plateau, the Andes, Greenland, and Antarctica, and seem to be proportional to the topographic height. The maximum coldness is over the Tibetan Plateau, up to −36°C, in June–August. However, the extent of cold biases is larger in December–February when the snow coverage is larger, and extends across most of eastern Asia. This could also be an effect of the Tibetan Plateau on the circulation that is not adequately modeled, but it is beyond the scope of this paper to determine. The coldness of the simulations in these regions is common to all the AMIP simulations, and could be due to too high snow-ice albedo or a deficiency in the calculation of surface heat flux on ice in the models. In the mountainous regions, stations are mostly located in valleys and the smoother model topography is always higher than the average elevation of the stations around the same grid point (M. Fennessy 1995, personal communication). Thus, the simulated surface air temperature would be slightly colder than the data. The scarcity of observations in the mountainous and permanent ice areas is another cause of large differences between the data and model simulations.

On the other hand, over the rest of the area of the continents, there are general warm biases of up to +12°C. These warm biases could be attributed to the

inadequate representation of land surface processes in the climate models. For example, the modeling experiments by Xue et al. (1996) showed that the significant warm biases over the central United States in NH summer in the COLA model are due to the erroneous prescription of crop vegetable phenology and crop soil properties in the surface parameterization of the GCM.

Zonal averages of the simulations show very good correspondence with the observations, except where the influences of the very cold Tibetan Plateau and Andes show in the annual mean and DJF means (Fig. 6). The one exception is over the Antarctic ice sheet, where the cold AMIP simulations are in contrast to previous results, which showed warm biases of GCM simulations (Houghton et al. 1990). Nevertheless, we are confident that there are insufficient validation data to draw strong conclusions over Antarctica.

b. Variability

Figure 7 shows the global mean anomalies of the data and the simulations, relative to their own 10-yr means. The general colder anomalies in the first three years and the last year are due to the shift of the SST forcing data, as mentioned above, but several of the NH winters show large differences between the simulations and observations. The model average for the winter of 1980/81 and at the very end of the run is notably colder than the data, whereas the simulations for the winter of 1984/85 are much warmer than the real world.

If the land air temperature patterns were controlled completely by the circulation patterns forced by SSTs and it is assumed that the models are perfect, there would be no differences between the modeled and observed temperature patterns over land. In smoothed monthly mean modeled and observed data, small differences would be expected due to weather noise, but the large winter excursions and 1982 NH summer differences call for an explanation. Here we examine three possibilities: response to forcing that is not included in

DJF modeled − observed surface air temperature
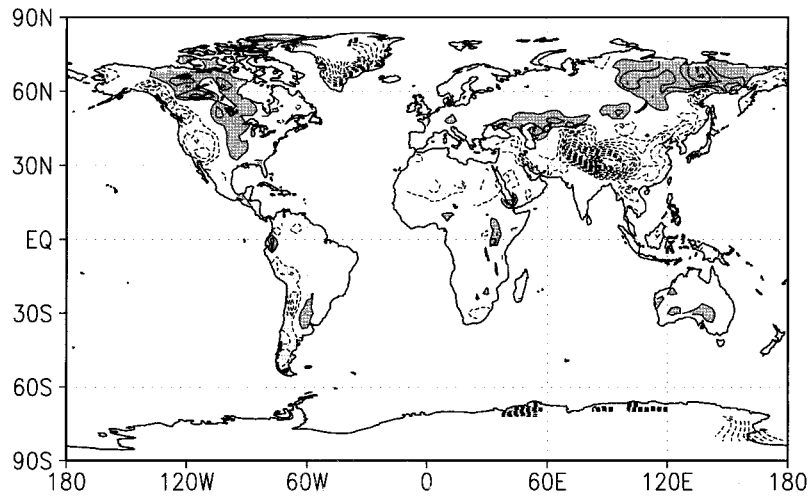
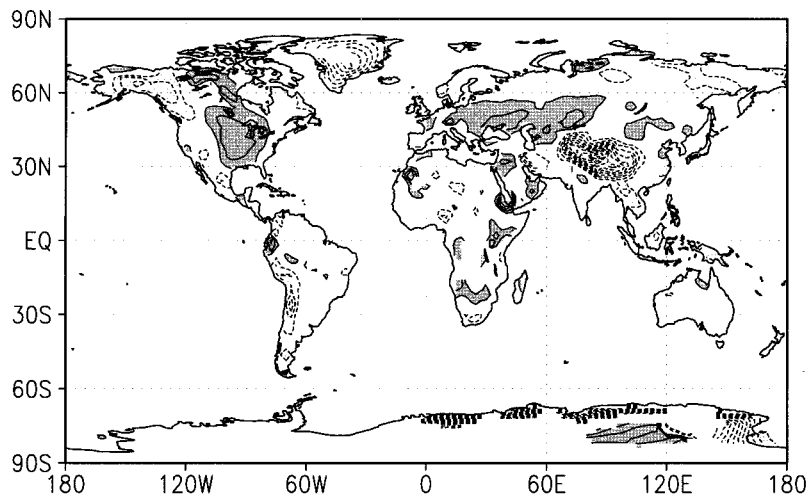## JJA modeled − observed surface air temperature

FIG. 5. Surface air temperature errors for December–February (DJF) (upper panel) and June–August (JJA) (bottom panel) for the average of the 16 selected simulations. Contour interval is 2°C. The values less than −2°C are shaded lightly, while values greater than 2°C are shaded darkly.

the AMIP design, in particular the April 1982 El Chichón volcanic eruption; inadequate remote model response to SST anomalies; and large internally generated circulation anomalies.

First, it seems that the extremely warm NH winters of 1980/81 and 1988/89 and the extremely cold winter of 1984/85, without any apparent external forcing, most likely resulted from internal mechanisms of the atmosphere. The AMIP simulations, on the contrary, show cold anomalies during the winters 1980/81 and 1988/89, and a warm anomaly during winter 1984/85. The biases of AMIP simulations during these three NH winters are confined to the mid- and high latitudes. As discussed by Barnett et al. (1997), it is not surprising that internally generated atmospheric variability of this scale

would occur during the AMIP period without any external forcing. Wallace et al. (1995) also point out a large dynamically induced component of internal variability in the observed surface temperature record, which is coherent across both NH continents in the cold season. This also means that all the explanations below, in which we attribute specific causes to the errors of the AMIP simulations, are subject to some uncertainty, as natural variability could always be a contributor to part of the differences (Hasselmann 1976; Robock 1978).

Nevertheless, we suggest that one possibility of the poor land air temperature simulation during the three extraordinary NH winters is the inadequate representation of the stratosphere and its interaction with the troposphere. Data analysis (Labitzke and van Loon
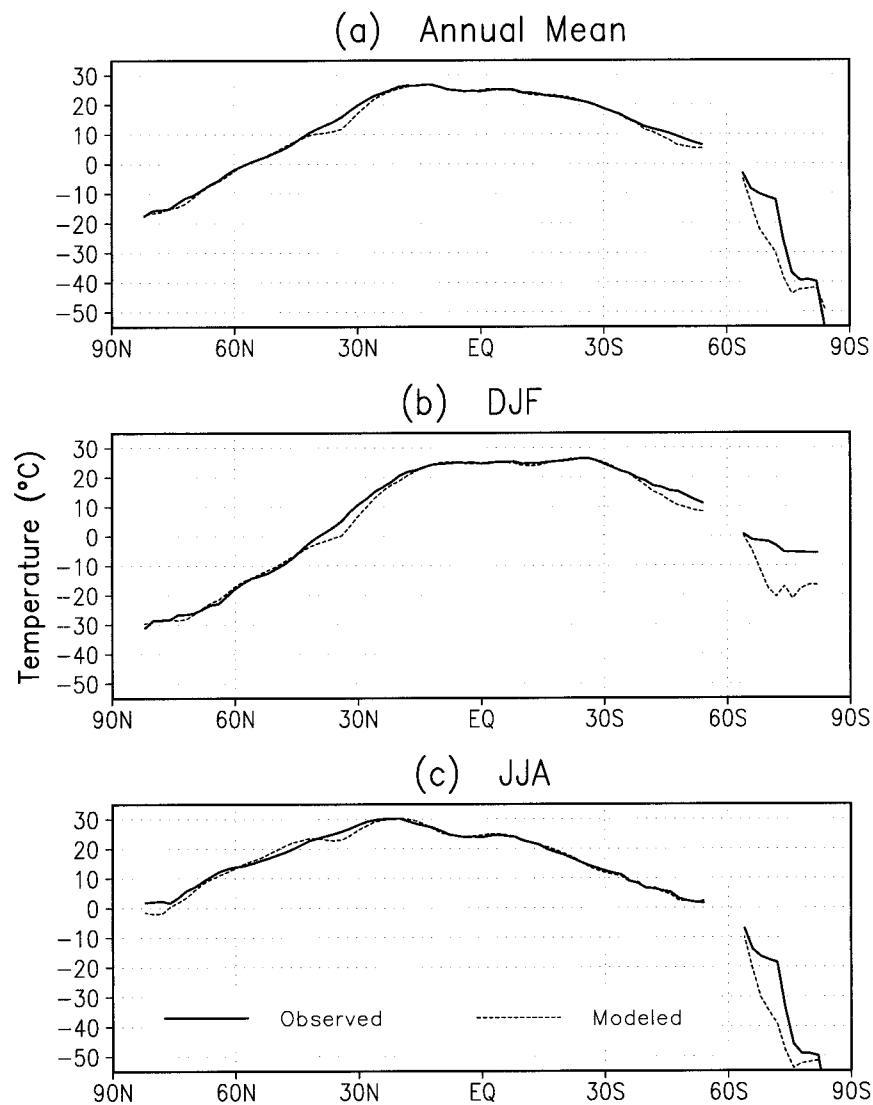
(a) Annual Mean

(b) DJF

(c) JJA

FIG. 6. The 1979–88 10-yr averaged zonal mean land air temperature for the data (solid line) and average of the 16 selected simulations (dashed line) for (a) annual mean, (b) DJF, and (c) JJA.

1988; Kodera 1994; Baldwin et al. 1994; Perlwitz and Graf 1995) and GCM experiments (Boville 1984; Graf et al. 1993) show that there are strong links between the stratospheric and tropospheric large-scale circulation anomalies during NH wintertime. The most dominant mode of these links is that in the NH there are positive geopotential height anomalies in the middle troposphere in the mid- and high latitudes and negative anomalies in the low latitudes and around the polar region when the NH stratospheric polar vortex is enhanced, and vice versa when the polar vortex is weaker. This baroclinic mode (shifting horizontally throughout the troposphere) corresponds to a major warming in the mid- and high latitudes and cooling in the low latitudes and polar region in the lower troposphere for a strong polar vortex, and vice versa for a weak polar vortex (Kodera 1994;

Perlwitz and Graf 1995). The three NH winters 1980/81, 1984/85 and 1988/89, all showing dominant temperature anomalies over northern mid- and high-latitude continents (not shown), are good examples of the interrelationship between the stratosphere and the troposphere and show the Wallace et al. (1995) pattern. As shown in Fig. 3 of Perlwitz and Graf (1995), the extremely warm 1980/81 winter had a strong stratospheric polar vortex, the extremely cold 1984/85 winter had a weak polar vortex, and the warm 1988/89 winter also had a strong polar vortex although the cold ENSO event tended to weaken the polar vortex (van Loon and Labitzke 1987; Labitzke and van Loon, 1989). However, there is no one-to-one correspondence between the stratospheric polar vortex and land surface air temperature anomalies during the 10-yr period. For example, the NH

Global Mean Land Air Temperature Anomalies
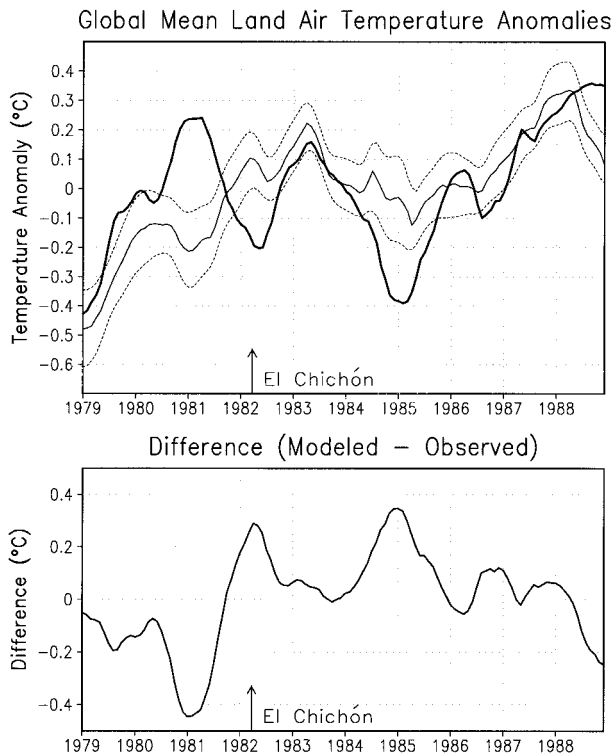

Difference (Modeled – Observed)

FIG. 7. Time series of low-pass-filtered globally averaged land temperature anomalies, relative to the 1979–88 period, for the data (thick solid line), average of the 16 selected simulations (thin solid line) and its values plus and minus one standard deviation of the 16 simulations (dashed lines) in the upper panel, and the difference between the two curves in the bottom panel. The years on the abscissa are plotted for January of the particular year.

winter 1987/88 with a weak stratospheric polar vortex was not anomalously cold over the NH continents. This means that, besides SST forcing and the stratospheric polar vortex, there are other significant factors governing the fluctuation of land surface air temperature, such as possible land surface processes and internal dynamic modes.

It is worth noting that the stratospheric polar vortex can be perturbed by external forcing (e.g., solar activity and volcanic eruptions), but also could be disturbed by natural internal variability. The mechanism of the interrelationship between the stratosphere and the troposphere will be described in detail in the last part of this section about the winter warming from the El Chichón eruption.

1) ENSO SIGNALS

The AMIP 10-yr simulations are forced by observed monthly mean SSTs, but use a fixed CO_2 concentration and solar constant, and no aerosol forcing. The change of solar radiation and concentrations of CO_2 and aerosols may have an influence on the fluctuation of observed SSTs, but for the 10-yr period, the largest SST

variations were ENSO events. Therefore, the major features of the simulated climate change during the period should be ENSO related.

ENSO is a result of complex air–sea interactions, characterized by large SST variations in the equatorial Pacific (Rasmusson and Carpenter 1982). ENSO causes a large fluctuation in the tropical atmosphere, and also links to some extratropical behavior of weather and climate (Horel and Wallace 1981; Hoskins and Karoly 1981). ENSO-related surface air temperature variations have been widely investigated (e.g., van Loon and Madden 1981), and some common patterns have been carefully documented (Halpert and Ropelewski 1992).

There has been considerable research on the atmospheric response to SST anomalies (e.g., Lau 1985; Lau and Nath 1990, 1996; Kumar et al. 1994). Teleconnection patterns associated with the anomalous tropical SSTs, such as the Pacific–North American pattern (PNA), have been simulated in various GCMs with some success (Held et al. 1989; Lau and Nath 1990; Kumar et al. 1994), and it is claimed that "atmospheric models are capable of giving a realistic simulation of the seasonal tropical atmospheric anomalies at least for intense El Niño periods if they are given a satisfactory estimate of the anomalous SST in the tropical Pacific" (Houghton et al. 1992, 121). GCMs previously, however, have been considered to have only a limited ability to simulate the atmospheric response to anomalous SSTs, especially for ENSO-related teleconnections in the extratropical regions (e.g., Zebiak 1986; Stendel and Bengtsson 1997). Here we take advantage of the AMIP experiment to see if the most up-to-date (as of the time of the AMIP runs) GCMs could actually do a good job of simulating the land response to SST variations.

Empirical orthogonal function (EOF) analysis of the 16 surface air temperature simulations showed various responses of land air temperature to SST anomalies. Some simulations present a clear and dominant ENSO mode for the 10-yr time series, but some do not. Thus, among these simulations we picked the eight best ones to represent the general ability of atmospheric GCMs to simulate the ENSO signal in the variability of surface air temperature. These eight simulations (CNRM, ECMWF, ECMWF2, GLA, JMA, NCAR, MPI, and NRL) have an ENSO mode that explains more than 15% of the total variance and has a correlation with the Southern Oscillation index (SOI; Chen 1982) of less than −0.7.

A rotated EOF analysis was performed on the average of the surface air temperature anomalies of the above eight simulations. (Unrotated EOF analysis gave a similar leading ENSO pattern.) Figure 8 shows the first EOF, which explains 29.5% of the total variance and has a correlation coefficient of −0.86 with the SOI at a 2-month lag. The negative correlation means that the surface air temperature has an above-normal anomaly when SOI is negative (warm mode), and below-normal anomaly when SOI is positive. This is obviously an
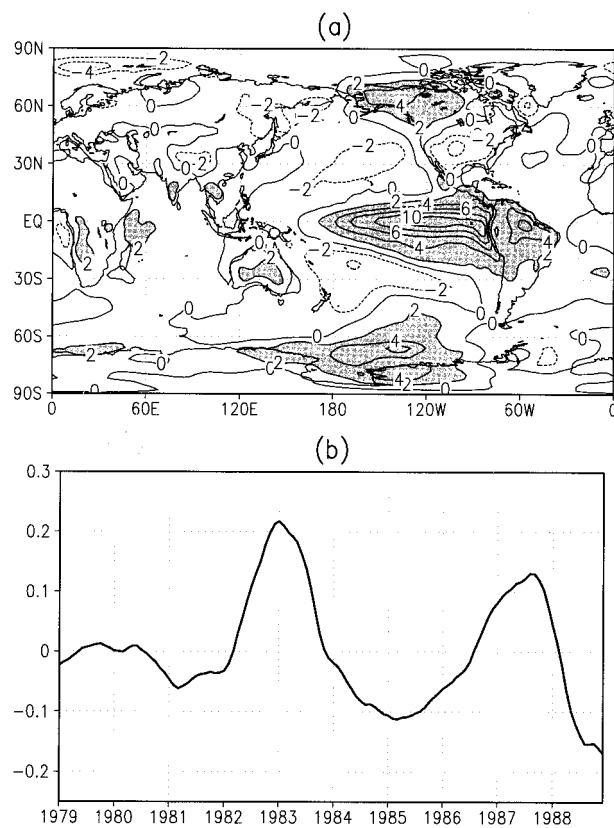
FIG. 8. First rotated EOF (a) and its principal component (b) of the average surface air temperature anomalies of the eight simulations with a strong ENSO signal. The years on the abscissa in (b) are plotted for January of the particular year.

FIG. 9. Same as Fig. 8 but for the second mode.

ENSO mode, corresponding to warm SST anomalies in the eastern equatorial Pacific and a compensating ''boomerang'' of cold SST anomalies in the central north and south Pacific for a warm ENSO episode, and the opposite pattern for a cold ENSO episode. It displays a PNA-like pattern over North America that is characterized by above-normal temperature anomalies over northwestern North America and below-normal anomalies over the southeastern United States. It also shows warm anomaly centers over southeastern Africa, southeastern Asia, central Australia, and South America. There are little signals over most of Eurasia. These simulated major ENSO-related features are consistent with those from a data composite by Halpert and Ropelewski (1992) and the SO–temperature correlation pattern calculated by Robock and Mao (1995). The centers over the Norwegian basin, Antarctica, and Tibetan Plateau are hard to verify because of insufficient data there. The signal over northeastern Asia was not clear in the data composite by Halpert and Ropelewski (1992), but was statistically significant in the correlation calculation by Robock and Mao (1995).

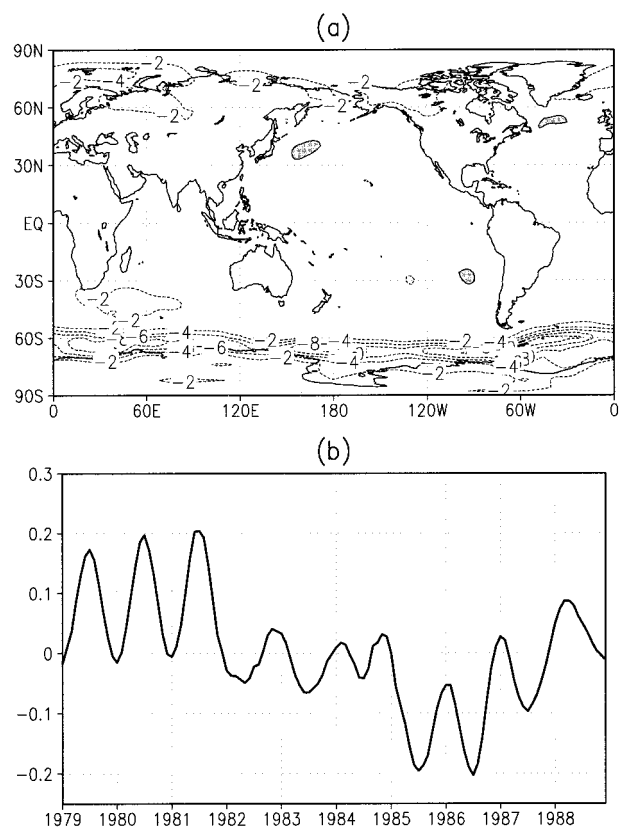It is interesting to note that the second (Fig. 9) and third mode (Fig. 10) of the rotated EOF analysis are obviously responses to the variation of sea-ice area in the Antarctic and Arctic, and explain 10.4% and 8.7% of the total variance, respectively. This result shows the significant effect of sea ice on NH mid- and high-latitude land surface air temperature fluctuations.

2) VOLCANIC COOLING

Dutton and Christy (1992) suggested that the temperature depression (in absolute terms in the observational record) during 1984–86 was a result of the cooling of the oceans by volcanic aerosols from the El Chichón eruption in 1982, and not an ENSO signal, because during that period the atmosphere did not present an ENSO-like circulation anomaly. However, it is not possible to evaluate this suggestion in the AMIP context, as the model simulations were forced by observed SSTs that had been influenced by El Chichón volcanic aerosols for the period. The simulations, however, certainly gave a weaker temperature depression during the period than observed.

During the period 1979–88, besides the three NH winters mentioned above, only summer 1982 has a large discrepancy between the data and simulations (shown in Fig. 7). We interpret the warm bias in the modeled temperature fluctuation as the result of the lack of volcanic aerosols from the El Chichón eruption in April 1982, in addition to those from the volcanic eruption of
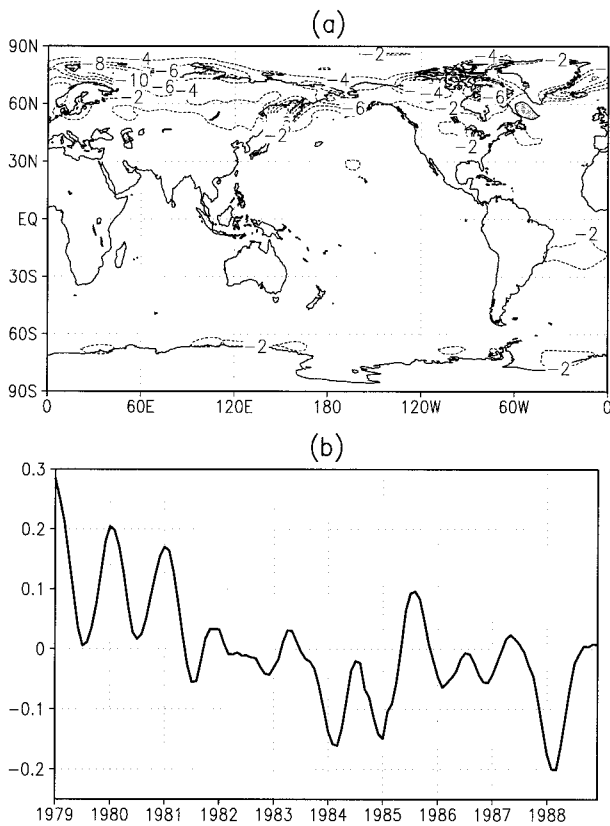
FIG. 10. Same as Fig. 8 but for the third mode.

Nyamuragira in December 1981 (Krueger et al. 1996). The dense stratospheric sulfate aerosols from the El Chichón eruption were able to block a significant amount of incoming sunlight and thus cooled the earth's surface and lower atmosphere (Robock 1983). Following the eruption, the monthly mean direct solar transmission observed at the Mauna Loa Observatory, Hawaii, decreased by as much as 14%, and the total solar radiation reduction was as much as 7% (Dutton and Christy 1992). This radiative forcing in the atmosphere is not included in the AMIP simulations. The land would cool faster than the oceans and, while a large amount of the volcanic cooling influence on SSTs would be realized in a few months after the volcanic eruption, the mixed layer of ocean would take several years to reach the new equilibrium. Therefore, the AMIP simulations could result in a warm bias over land in the first few months after volcanic eruptions due to the lack of the volcanic forcing.

Figure 7 shows a warm bias starting in 1981, before the Nyamuragira and El Chichón eruptions, because of the unrealistic climate drift from 1981 to 1982 due to the inhomogeneous SST datasets used in the model simulations, as discussed in the previous section, and the smoothing used in the figure. Volcanic cooling effects are usually estimated as the temperature following the eruption subtracted from the mean temperature in a pe-

riod (e.g., 5 yr) before the eruption when there is no other volcanic eruption. Therefore, this drift, without adequate adjustment, makes the quantitative estimate of the El Chichón global cooling effect impossible. Nevertheless, as the warm bias peaked in April–May 1982, it is indicative of an El Chichón global cooling effect. AMIP II, which will use a homogenous reanalysis of SSTs, will eliminate this drift and will let us make a clearer evaluation of the El Chichón signal.

3) WINTER WARMING FROM THE EL CHICHÓN ERUPTION

Robock and Mao (1992, 1995), using Jones surface temperature anomaly data (Jones et al. 1986a; Jones et al. 1986b), found a statistically significant major winter warming pattern over northern continents following the 12 largest historical volcanic eruptions since the Krakatau eruption in 1883. This regional and seasonal pattern is characterized by above-normal temperature anomalies over northern Eurasia, the United States, and southern Canada, and below-normal temperature anomalies over northern Canada, Greenland, North Africa, and the Middle East [see Fig. 12 of Robock and Mao (1995)].

A large volcanic eruption injects large amounts of SO_2 into the lower stratosphere, which is converted into submicron H_2SO_4 aerosols with a typical lifetime of 2–3 yr. The most obvious impact is to scatter some of the incoming solar radiation, producing cooling at the earth's surface that lasts for about 2 yr and has a maximum over land in the summer of the year following the eruption (Robock and Mao 1995). On the other hand, the volcanic aerosols absorb radiation, both in the solar near-infrared and terrestrial infrared wavelengths (Stenchikov et al. 1997), thus heating the atmosphere there (Quiroz 1983). The stratospheric warming by volcanic aerosols is proportional to the optical depth of the aerosols and radiation reaching the aerosol layer. In the NH winter (DJF), the warming is larger in low latitudes and less in the high latitudes (Labitzke and Naujokat 1983; Labitzke and McCormick 1992). Thus, the differential heating produces a larger pole-to-equator temperature gradient, which in turn increases the zonal winds and enhances the stratospheric polar vortex. The stronger polar vortex may affect the vertically propagating tropospheric planetary waves and thus modify the tropospheric circulation and then alter surface air temperature. This mechanism has been suggested by GCM calculations (Graf et al. 1993) and data analysis (Kodera 1994; Kodera and Yamazaki 1994). As a result, the North Atlantic Oscillation (NAO) is amplified (Baldwin et al. 1994; Perlwitz and Graf 1995; Mao 1995), and low-level thermal advection in the Atlantic region is modified to produce the surface air temperature anomaly pattern described above.

In the surface air temperature anomaly field, the NH winter 1982/83 was characterized by a major warming over northern Eurasia and southern North America and
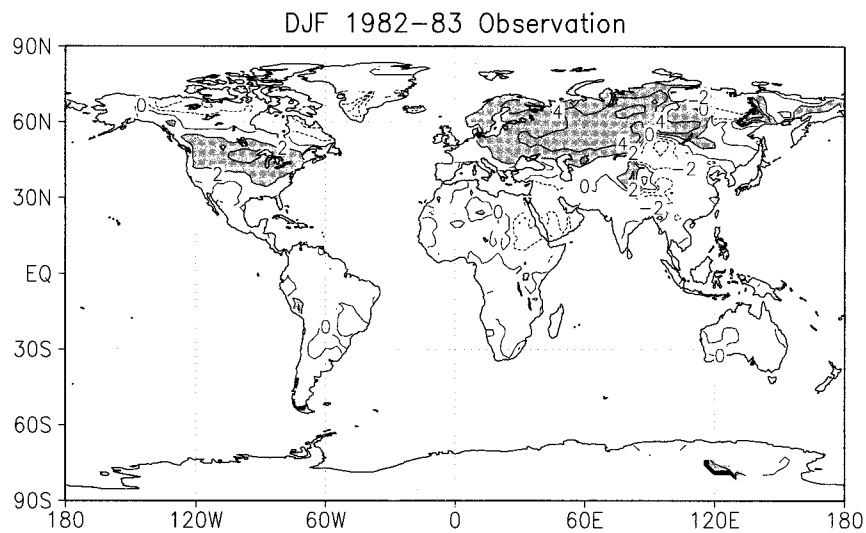
FIG. 11. DJF 1982/83 observed surface air temperature anomalies relative to the 1979–88 period. Anomalies larger than 1°C are shaded darkly, and anomalies less than −1°C are shaded lightly. The contour interval is 2°C.

cooling over northern Canada, the Middle East, and southeastern Asia (Fig. 11), which is similar to the winter warming pattern attributed to a large volcanic eruption (Robock and Mao 1992, 1995). However, for this particular case, the possibility that the coincident largest El Niño of the century produced these anomalies cannot be simply excluded. Although the ENSO signal was removed by a linear regression method in the results presented by Robock and Mao (1992, 1995), an ENSO is generated by nonlinear air–sea interaction and nonlinear components of the ENSO signal probably still remained in those results. In addition, there are often important differences in the characteristics and evolution of individual ENSO events. The extraordinary El Niño might have caused exceptional surface air temperature anomalies in the extratropics.

This sensitive and interesting issue can be tested by comparison between the AMIP simulated ENSO signals and the data. Forced by observed SSTs, the AMIP simulations of surface air temperature can tell if the observed anomaly pattern during NH winter 1982/83 is produced by ENSO or not. Looking at the simulated dominant ENSO mode in Fig. 8, we can see clearly that the major warming over northern Eurasia during the NH winter 1982/83 (Fig. 11) is not related to ENSO, and the pattern over North America is totally opposite to the ENSO mode. There are above-normal temperature anomalies over southern North America and below-normal anomalies over northern North America in the data (Fig. 12a), but the simulations (Fig. 12b) show above-normal anomalies over northern North America and below-normal anomalies over southern North America. Compared to the composite ENSO signal from historical data (Halpert and Ropelewski 1992) and the typical NH winter warming pattern following historical volcanic

eruptions (Robock and Mao 1992, 1995), the 1982/83 NH winter surface air temperature anomaly pattern (Fig. 11) is not ENSO like, at least not typically ENSO like, but most likely a typical volcanic winter warming pattern. The field correlation between the data and the mean of simulations over the North American (24°–76°N, 50°–170°W) continent is −0.57 for NH winter 1982/83. Following the 1986–87 El Niño, however, without a coincident volcanic eruption, the 1986/87 NH winter simulation pattern (Fig. 12d) resembles the observations (Fig. 12c) and has a +0.47 field correlation. These findings give support to our previous results (Robock and Mao 1992, 1995), further strengthening the volcanic winter warming theory.

4. Discussion and conclusions

Thirty available AMIP simulations of 1979–88 surface air temperature are analyzed and compared with observations. The comparison between the simulations and the data is made only over land because the temperatures are specified over the oceans in the AMIP experimental design. With a boundary forcing of observed monthly mean SSTs, most of the simulations gave a rather realistic seasonal cycle of the global mean of land air temperature. The simulated mean climate has a general cold bias compared to the observations, which implies that most of the models suffer from a common deficiency in some aspects of their formulation, despite the marked differences in resolution and the diversity of their physical parameterizations. The general coldness of the models is larger from NH winter to early summer than the rest of the year.

Every model shows the largest cold biases in the mountain areas and over permanent ice, with a maxi-
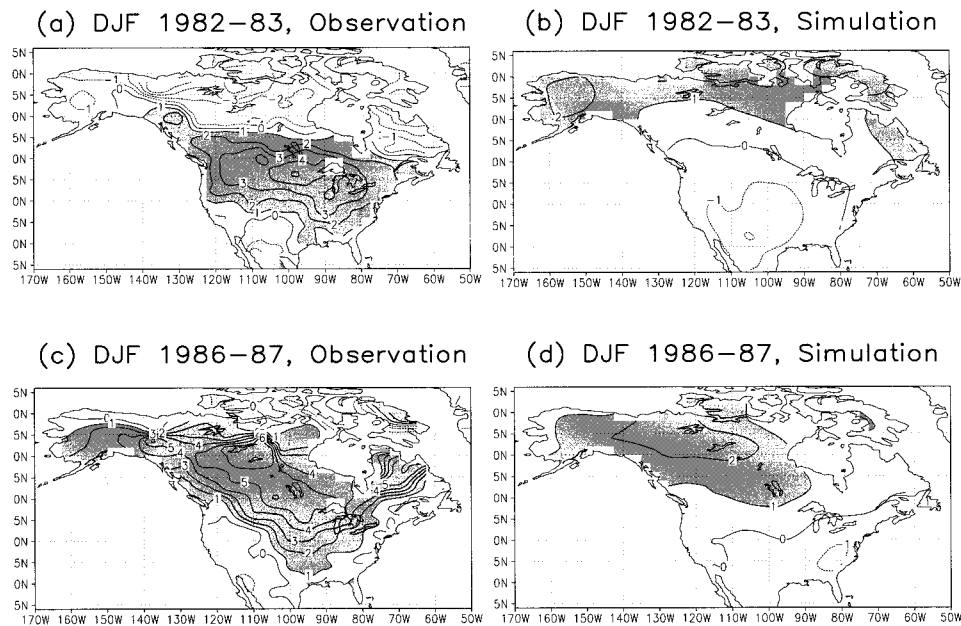
FIG. 12. Surface air temperature anomalies over North America for DJF 1982/83 and DJF 1986/87. The observations are obtained from Schemm et al. (1992), and the simulation is the average of the eight best AMIP simulations for the ENSO signal. Positive anomalies larger than 0.5°C are shaded darkly, and negative anomalies less than −0.5°C are shaded lightly. The contour interval is 1°C.

mum over the Tibetan Plateau. This feature may be associated with too high snow-ice albedo, or due to the difference between model topography and station height. The insufficient data coverage in these regions might be another reason for the large biases. The large biases in the mountain areas might also reflect the deficiency of current GCMs' resolution in the areas where the temperature gradient is extremely large. In contrast, in the middle of the continents there are general warm biases. In summer, the biases could be attributed to the improper representation of land surface properties. Apparently, there are many factors closely influencing the surface air temperature simulation in a GCM, such as snow treatment, prescribed surface albedo, the planetary boundary layer, and soil moisture. Further work is desired to understand the models' deficiency in surface air temperature simulation in detail by analyzing other related AMIP outputs, for example, surface heat flux and snow coverage (D. Randall 1995, personal communication).

Using climatological SSTs outside 40°S–50°N for 1979–81 with a larger sea ice area as the boundary forcing of the AMIP simulations resulted in a colder mean climate of land air temperature simulations in high latitudes, compared to the rest of years in the period. The influence of the shift of SST forcing data has complicated the analysis of AMIP results, especially in land surface air temperature, which has a close relationship to the forcing data over oceans. This drift could be eliminated by using a reanalysis of SSTs in the future.

The ENSO mode is the dominant mode in the inter-annual variability of the simulations. Eight among the sixteen simulations with a realistic global-mean climate present an evident ENSO mode. On the average, the ENSO mode explains about 30% of the total variance and has a 2-month lag with respect to the SOI, an indicator of the Walker circulation anomaly in the atmosphere. The variance explained by the ENSO mode is equivalent to that explained by the linear regression relationship between the SOI and the high-frequency surface air temperature anomalies based on historical data back to 1886 (Robock and Mao 1995), although the model simulations contain less variability than the data. The ENSO signal over land is smaller than the data in amplitude but its pattern is in good agreement with previous data composites.

Currently, direct calculation of volcanic effects on the climate is uncertain (Hansen et al. 1992) because of insufficient measurements of microphysical and optical properties of volcanic aerosols, in addition to improper representation of their radiative forcing and thermodynamic and dynamic responses of climate system. In addition, the coincident 1982/83 El Niño complicated the detection of the influence of El Chichón eruption in April 1982. The AMIP experiment provided a unique opportunity and indirect way of detecting the volcanic signal by looking at the contrast between the data and the simulations, due to the lack of volcanic forcing in the model calculations. A warm bias of the model simulations as compared with the data peaked in the first 2 months after the El Chichón eruption suggesting an El Chichón cooling effect enhancing the cooling after

the Nyamuragira eruption in December 1981. However, the mean climate shift due to SST forcing data discontinuity at the end of 1981 made a quantitative estimate of the El Chichón global cooling influence impossible in this experiment. Regionally, the comparison of the simulations with data suggests that the major warming over the North American and Eurasian continents in the 1982/83 NH winter is not an ENSO-dominant mode, but rather a pattern associated with the enhanced stratospheric polar vortex by the larger equator-to-pole temperature gradient produced by volcanic sulfate aerosols in the stratosphere.

These results validate the design of the AMIP experiment and show that, while models can give valuable information about the causes of climate change of the 10 yr from 1979 to 1988, there is still much room for improvement in atmospheric climate models. Only half of the AMIP calculations even produced simulations of land air temperature close to observations, even though they were forced with observed surface temperatures over 70% of the planet. And only half of the remaining models produced reasonable ENSO simulations, and those simulations did not produce extratropical patterns of the correct amplitude. It is beyond the scope of this paper to diagnose the reasons for these disagreements, but continuous improvement in model resolution and physical parameterizations should improve these simulations. Nevertheless, it should be emphasized that the results may not be indicative of current model versions. For example, a new version of the CSU model has introduced SiB2 (Sellers et al. 1996), which has made a big improvement in the surface air temperature simulation (Randall et al. 1996), compared to the bucket model used in the AMIP run. We look forward to future AMIP experiments, which use improved models and include the 1991 Pinatubo eruption to further examine the volcanic signal in surface air temperatures.

The major difference between the observation and the model simulations is during the NH wintertime. The fundamental reason is that the interannual NH winter temperature anomalies are more chaotic (contain more components of natural internally generated variability of the atmosphere) than during the rest of the year. The good correspondence of the observed land temperature fluctuations and stratospheric polar vortex for both years with and without volcanic eruptions suggests that the interaction between the stratosphere and the troposphere is an important mode of the internal variability of land air temperature. Current GCMs have large deficiencies in simulating stratospheric processes (e.g., QBO) and their interactions with the troposphere. We suggest that an emphasis on improvement in the simulation of the radiative and dynamical links between the stratosphere and troposphere would go a long way to improve climate model simulations of the surface response to climate forcing.

REFERENCES

Baldwin, M., X. Cheng, and T. J. Dunkerton, 1994: Observed correlations between winter-mean tropospheric and stratospheric circulation anomalies. *Geophys. Res. Lett.,* **21,** 1141–1144.

Barnett, T., K. Arpe, L. Bengtsson, M. Ji, and A. Kumar, 1997: Potential predictability and AMIP implications of midlatitude climate variability in two general circulation models. *J. Climate,* **10,** 2321–2329.

Boer, G. J., and Coauthors, 1992: Some results from an intercomparison of the climates simulated by 14 atmospheric general circulation models. *J. Geophys. Res.,* **97,** 12 771–12 786.

Boville, B. A., 1984: The influence of polar night jet on the tropospheric circulation in a GCM. *J. Atmos. Sci.,* **41,** 1132–1142.

Chen, W. Y., 1982: Assessment of Southern Oscillation sea level pressure indices. *Mon. Wea. Rev.,* **110,** 800–807.

Dutton, E. G., and J. R. Christy, 1992: Solar radiative forcing at selected locations and evidence for global lower tropospheric cooling following the eruptions of El Chichón and Pinatubo. *Geophys. Res. Lett.,* **19,** 2313–2316.

Gates, W. L., 1992a: AMIP: The Atmospheric Model Intercomparison Project. *Bull. Amer. Meteor. Soc.,* **73,** 1962–1970.

——, 1992b: *AMIP Newsletter No. 2.* Lawrence Livermore National Laboratory, 8 pp.

——, 1994: *AMIP Newsletter No. 5.* Lawrence Livermore National Laboratory, 16 pp.

Graf, H. F., I. Kirchner, A. Robock, and I. Schult, 1993: Pinatubo eruption winter climate effects: Model versus observations. *Climate Dyn.,* **9,** 81–93.

Halpert, M. S., and C. F. Ropelewski, 1992: Surface temperature patterns associated with the Southern Oscillation. *J. Climate,* **5,** 577–593.

Hansen, J. E., A. Lacis, R. Ruedy, and M. Sato, 1992: Potential climate impact of Mount Pinatubo eruption. *Geophys. Res. Lett.,* **19,** 215–218.

——, and Coauthors, 1996: A Pinatubo climate modeling investigation. *The Mount Pinatubo Eruption,* G. Fiocco, D. Fuà, and G. Visconti, Eds., NATO ASI Series, No. 42, Springer-Verlag, 233–272.

Hasselmann, K., 1976: Stochastic climate models. Part 1: Theory. *Tellus,* **28,** 473–485.

Held, I. M., S. W. Lyons, and S. Nigam, 1989: Transients and the extratropical response to El Niño. *J. Atmos. Sci.,* **46,** 163–174.

Horel, J. D., and J. M. Wallace, 1981: Planetary-scale atmospheric phenomena associated with the Southern Oscillation. *Mon. Wea. Rev.,* **109,** 813–829.

Hoskins, B. J., and D. J. Karoly, 1981: The steady linear response of a spherical atmosphere to thermal and orographic forcing. *J. Atmos. Sci.,* **38,** 1179–1196.

Houghton, J. T., G. J. Jenkins, and J. J. Ephraums, Eds., 1990: *Climate Change, The IPCC Scientific Assessment.* Cambridge University Press, 365 pp.

——, B. A. Callander, and S. K. Varney, Eds., 1992: *Climate Change 1992, The Supplementary Report to The IPCC Scientific Assessment.* Cambridge University Press, 196 pp.

Jones, P. D., S. C. B. Raper, R. S. Bradley, H. F. Diaz, P. M. Kelly, and T. M. L. Wigley, 1986a: Northern Hemisphere surface air temperature variations: 1851–1984. *J. Climate Appl. Meteor.,* **25,** 161–179.

——, ——, and T. M. L. Wigley, 1986b: Southern Hemisphere surface air temperature variations: 1851–1984. *J. Climate Appl. Meteor.,* **25,** 1213–1230.

Kodera, K., 1994: Influence of volcanic eruptions on the troposphere through stratospheric dynamical processes in the Northern Hemisphere. *J. Geophys. Res.,* **99,** 1273–1282.

——, and K. Yamazaki, 1994: A possible influence of recent polar stratospheric coolings on the troposphere in the Northern Hemisphere winter. *Geophys. Res. Lett.,* **21,** 809–812.

Krueger, A., C. Schnetzler, and L. Walter, 1996: The December 1981 eruption of Nyamuragira Volcano (Zaire), and the origin of the "mystery cloud" of early 1982. *J. Geophys. Res.,* **101,** 15 191–15 196.

Kumar, A., A. Leetmaa, and M. Ji, 1994: Simulations of atmospheric variability induced by sea surface temperatures and implications for global warming. *Science,* **266,** 632–634.

Labitzke, K., and B. Naujokat, 1983: On the variability and on trends of the temperature in the middle stratosphere. *Contrib. Atmos. Phys.,* **56,** 495–507.

——, and H. van Loon, 1988: Association between the 11-year solar cycle, the QBO, and the atmosphere. Part I: The troposphere and the stratosphere in the Northern Hemisphere in winter. *J. Atmos. Terr. Phys.,* **50,** 197–206.

——, and M. P. McCormick, 1992: Stratospheric temperature increases due to Pinatubo aerosols. *Geophys. Res. Lett.,* **19,** 207–210.

Lacis, A. A., J. E. Hansen, and M. Sato, 1992: Climate forcing by stratospheric aerosols. *Geophys. Res. Lett.,* **19,** 1607–1610.

Lau, N.-C., 1985: Modeling the seasonal dependence of the atmospheric response to observed El Niño in 1962–76. *Mon. Wea. Rev.,* **113,** 1970–1996.

——, and M. J. Nath, 1990: A general circulation model study of the atmospheric response to extratropical SST anomalies observed in 1950–79. *J. Climate,* **3,** 965–989.

——, and ——, 1996: The role of the "atmospheric bridge" in linking tropical Pacific ENSO events to extratropical SST anomalies. *J. Climate,* **9,** 2036–2057.

Mao, J., 1995: Effects of volcanic eruptions on climate: Signal detection in surface temperature observations. Ph.D. dissertation, University of Maryland at College Park, 119 pp. [Available from Dept. of Meteorology, University of Maryland, College Park, MD 20742.]

——, and A. Robock, 1995: Report of AMIP Diagnostic Subproject 19. Part 2: The surface air temperature record in the AMIP simulations and the influence of El Chichón. *Proc. First Int. AMIP Scientific Conf.,* Monterey, CA, WCRP-92, WMO/TD-No. 732, 471–476.

Perlwitz, J., and H. F. Graf, 1995: The statistical connection between troposphere and stratosphere circulation of the Northern Hemisphere in winter. *J. Climate,* **8,** 2281–2295.

Phillips, T. J., 1994: A summary documentation of the AMIP models. PCMDI Rep. No. 18, Lawrence Livermore National Laboratory, 343 pp. [Available from National Technical Information Service, U.S. Department of Commerce, 5285 Port Royal Rd., Springfield, VA 22161.]

Quiroz, R. S., 1983: The isolation of stratospheric temperature change

due to the El Chichón volcanic eruption from nonvolcanic signals. *J. Geophys. Res.,* **88,** 6773–6780.

Rampino, M. R., and S. Self, 1984: Sulphur-rich volcanic eruptions and stratospheric aerosols. *Nature,* **310,** 677–679.

Randall, D. A., and Coauthors, 1996: A revised land–surface parameterization (SiB2) for atmospheric GCMs. Part III: The greening of the CSU general circulation model. *J. Climate,* **9,** 738–763.

Rasmusson, E. M., and T. H. Carpenter, 1982: Variations in tropical sea surface temperature and surface wind fields associated with the Southern Oscillation/El Niño. *Mon. Wea. Rev.,* **110,** 354–384.

Reynolds, R. W., 1988: A real-time global sea surface temperature analysis. *J. Climate,* **1,** 75–86.

Robock, A., 1978: Internally and externally caused climate change. *J. Atmos. Sci.,* **35,** 1111–1122.

——, 1983: The dust cloud of the century. *Nature,* **301,** 373–374.

——, 1984: Climate model simulations of the effects of the El Chichón eruption. *Geofis. Int.,* **23,** 403–414.

——, and J. Mao, 1992: Winter warming from large volcanic eruptions. *Geophys. Res. Lett.,* **19,** 2405–2408.

——, and ——, 1995: The volcanic signal in surface temperature observations. *J. Climate,* **8,** 1086–1103.

——, C. A. Schlosser, K. Y. Vinnikov, N. A. Speranskaya, and J. K. Eutin, 1998: Evaluation of AMIP soil moisture simulations. *Global Planet. Change,* in press.

Schemm, J., S. Schubert, J. Terry, and S. Bloom, 1992: Estimate of monthly mean soil moisture for 1979–89. NASA Tech. Memo. 104571, 252 pp. [Available from National Technical Information Service, U.S. Department of Commerce, 5285 Port Royal Rd., Springfield, VA 22161.]

Sellers, P. J., D. A. Randall, G. J. Collatz, J. Berry, C. Field, D. A. Dazlich, C. Zhang, and L. Bounoua, 1996: A revised land–surface parameterization (SiB2) for atmospheric GCMs. Part I: Model formulation. *J. Climate,* **9,** 706–737.

Spangler, W. M. L., and R. L. Jenne, 1990: World monthly surface station climatology. National Center for Atmospheric Research. [Available from Data Support Section, Scientific Computing Division, NCAR, Box 3000, Boulder, CO 80307.]

Spencer, R. W., and J. R. Christy, 1993: Precision lower stratospheric temperature monitoring with the MSU: Technique, validation, and results 1979–1991. *J. Climate,* **6,** 1194–1204.

Stenchikov, G. L., I. Kirchner, A. Robock, H.-F. Graf, J. C. Antuña, R. G. Grainger, A. Lambert, and L. Thomason, 1997: Radiative forcing from the 1991 Mount Pinatubo volcanic eruption. Max-Planck Inst. for Meteor. Rep. 231, 40 pp. [Available from Max-Planck-Institut für Meteorologie, Bundesstrasse 55, D-20146 Hamburg, Germany.]

Stendel, M., and L. Bengtsson, 1997: Toward monitoring the tropospheric temperature by means of a general circulation model. *J. Geophys. Res.,* **102,** 29 779–29 788.

van Loon, H., and R. Madden, 1981: The Southern Oscillation. Part I: Global associations with pressure and temperature in northern winter. *Mon. Wea. Rev.,* **109,** 1150–1162.

——, and K. Labitzke, 1987: The Southern Oscillation. Part V: The anomalies in the lower stratosphere of the Northern Hemisphere in winter and a comparison with the quasi-biennial oscillation. *Mon. Wea. Rev.,* **115,** 357–369.

Wallace, J. M., Y. Zhang, and J. A. Renwick, 1995: Dynamic contribution to hemispheric mean temperature trends. *Science,* **270,** 780–783.

Xue, Y., M. Fennessy, and P. Sellers, 1996: Impact of vegetation properties on U.S. summer weather prediction. *J. Geophys. Res.,* **101,** 7419–7430.

Zebiak, S. E., 1986: Atmospheric convergence feedback in a simple model for El Niño. *Mon. Wea. Rev.,* **114,** 1263–1271.